https://doi.org/10.5194/egusphere-2024-1846
Preprint. Discussion started: 18 July 2024

Technical note: Towards atmospheric compound identification in chemical ionization mass spectrometry with machine learning

Federica Bortolussi[1], Hilda Sandström[2], Fariba Partovi[3,4], Joona Mikkilä[4], Patrick Rinke[2,5,6], and Matti Rissanen[1,3]

[1]Department of Chemistry, University of Helsinki, 00560 Helsinki, Finland
[2]Department of Applied Physics, Aalto University, Espoo, Finland
[3]Aerosol Physics Laboratory, Physics Unit, Tampere University, 33720 Tampere, Finland
[4]Karsa Ltd., A. I. Virtasen aukio 1, 00560 Helsinki, Finland
[5]Physics Department, TUM School of Natural Sciences, Technical University of Munich, Garching, Germany
[6]Atomistic Modelling Center, Munich Data Science Institute, Technical University of Munich, Garching, Germany

Correspondence: Federica Bortolussi (federica.bortolussi@helsinki.fi)

Abstract.

Chemical ionization mass spectrometry (CIMS) is widely used in atmospheric chemistry studies. However, due to the complex interactions between reagent ions and target compounds, chemical understanding remains limited and compound identification difficult. In this study, we apply machine learning to a reference dataset of pesticides in two standard solutions to build a model that can provide insights from CIMS analyses in atmospheric science. The CIMS measurements were performed with an orbitrap mass spectrometer coupled to a thermal desorption multi-scheme chemical ionization inlet unit (TD-MION-MS) with both negative and positive ionization modes utilizing Br^-, $O_2{}^-$, H_3O^+ and $(CH_3)_2COH^+$ ($AceH^+$) as reagent ions. We then trained two machine learning methods on this data: 1) random forest (RF) for classifying if a pesticide can be detected with CIMS, and 2) kernel ridge regression (KRR) for predicting the expected CIMS signals. We compared their performance on five different representations of the molecular structure: the topological fingerprint (TopFP), the molecular access system keys (MACCS), a custom descriptor based on standard molecular properties (RDKitPROP), the Coulomb matrix (CM) and the many-body tensor representation (MBTR). The results indicate that MACCS outperforms the other descriptors. Our best classification model reaches a prediction accuracy of 0.85 ± 0.02 and a receiver operating characteristic curve area of 0.91 ± 0.01. Our best regression model reaches an accuracy of 0.44 ± 0.03 logarithmic units of the signal intensity. Subsequent feature importance analysis of the classifiers reveals that the most important structural fragments are NH and OH for the negative ionization schemes and nitrogen-containing groups for the positive ionization schemes.

1 Introduction

Mass spectrometry (MS) is an analytical technique for molecular compound identification and tracking in a variety of fields (e.g. biochemistry, food control, forensic science, pollution control, reaction physics and kinetics, thermodynamic parameters determination) (Griffiths and de Hoffmann, 2007). In atmospheric science, chemical ionization mass spectrometry (CIMS) has proliferated, because it can detect gas-phase compounds at atmospheric pressures (Sipilä et al., 2016; Laskin et al., 2018;

https://doi.org/10.5194/egusphere-2024-1846
Preprint. Discussion started: 18 July 2024

Huey, 2007; Eisele and Tanner, 1993; Munson, 1971; Munson and Field, 1966; Riva et al., 2019; Breitenlechner et al., 2017; de Gouw and Warneke, 2007). CIMS' low detection limit, good sensitivity, low probability of fragmentation and the ability to detect charged volatile compounds, make it an ideal compound tracking technique, but compound identification remains challenging. Multi-scheme chemical ionization inlets (MIONs) (Rissanen et al., 2019) provide more information than single ionization schemes. However, our understanding of the complex interaction between reagent ions and sample molecules is still too limited to routinely identify compounds from CIMS spectra (Munson, 2006; Sandström et al., 2023).

To improve compound identification, quantum chemical calculations are used to model the interaction between reagent ions and target molecules. Early breakthroughs revealed a correlation between the binding energy (between reagent ion and target molecule) and the experimental detection sensitivity (Partovi et al., 2023, 2024b; Iyer et al., 2016; Hyttinen et al., 2018). However, due to the high complexity of the interaction, the large configuration space of possible ion-molecule structures and the cost of the quantum chemical calculations, databases are challenging to produce. Thus no compound identification workflow has emerged so far.

In this article, we explore if purely data-driven machine learning (ML) can facilitate CIMS compound identification. ML excels at pattern identification, data-driven classification and regression tasks. ML is proliferating in the natural sciences and has started to emerge in atmospheric science for, e.g., physicochemical property prediction (Lumiaro et al., 2021; Besel et al., 2023), detection of new particle formation events (Su et al., 2022), boundary layer height estimation (Krishnamurthy et al., 2021), or aerosol classification (Siomos et al., 2020). In other chemical domains, e.g. metabolomics, ML has successfully enabled chemical compound identification from fragmentation mass spectrometry (Erban et al., 2019; Heinonen et al., 2012; Dührkop et al., 2015; Brouard et al., 2016; Nguyen et al., 2018, 2019). In atmospheric science, the lack of data and data standards has prevented a similar development for CIMS or fragmentation mass spectrometry (Sandström et al., 2023; Thoma et al., 2022).

In this work, we address the data scarcity with a new dataset of CIMS spectra containing pesticides. Pesticides constitute only a minor fraction of atmospheric compounds (Brüggemann et al., 2024; Houde et al., 2019), but are available as standard solutions from chemical suppliers. The dataset, therefore, provides CIMS spectra for approximately 700 clearly defined reference molecules. This data volume is similar to what was used in metabolomics to build the first ML compound identification tools (Heinonen et al., 2012; Dührkop et al., 2015; Brouard et al., 2016; Nguyen et al., 2018, 2019).

Our objective in this work is to develop ML models that learn the relation between CIMS spectra and their corresponding compounds. Specifically, we will investigate, if we can predict a pesticide detection by CIMS, and further, if we can predict the resulting signal intensity of different ionization methods from the atomic structure of a pesticide molecule. Such predictions could be used prior to deployment (e.g., in a field measurement campaign or for pesticide detection and monitoring) to ensure that the detector is appropriate and sensitive enough. The ML methods will also provide insight into the interaction between reagent ions and molecules which will help us to develop future compound identification methods in atmospheric science.

Figure 1 presents a schematic ML workflow followed in this work. The measurements were carried out with a thermal desorption (TD) MION-MS, and the experiments were run sequentially with four different ionization schemes: Br^-, $O_2{}^-$, H_3O^+ and $(CH_3)_2COH^+$ ($AceH^+$). The dataset is then preprocessed and used for training two ML algorithms: random forests

https://doi.org/10.5194/egusphere-2024-1846
Preprint. Discussion started: 18 July 2024

(RF) (Breiman, 2001) for detection classification and a kernel ridge regression (KRR) (Rupp, 2015) models to predict CIMS signal intensities of a given pesticide. The models are trained on different molecular descriptors that encode the structural and chemical features of each pesticide. We tested five different representations: properties obtained from the pesticides' structure (RDKitPROP), the topological fingerprint (TopFP) (James et al., 1995), the molecular access system keys (MACCS) (Durant et al., 2002), the Coulomb matrix (CM) (Rupp et al., 2012) and the many-body tensor representation (MBTR) (Huo and Rupp, 2022). Since the descriptors differ in their complexity and explainability, we compared their performance for both classification and regression.

The manuscript is organized as follows: Sect. 2 presents the dataset used in this work. Sect. 3 and Sect. 4 introduce the molecular descriptors and ML methodology, respectively. Sect. 5 presents the results of the classification (Sect. 5.1) and regression (Sect. 5.2) models, as well as a discussion on the chemical insight gained from the ML models (Sect. 5.3).

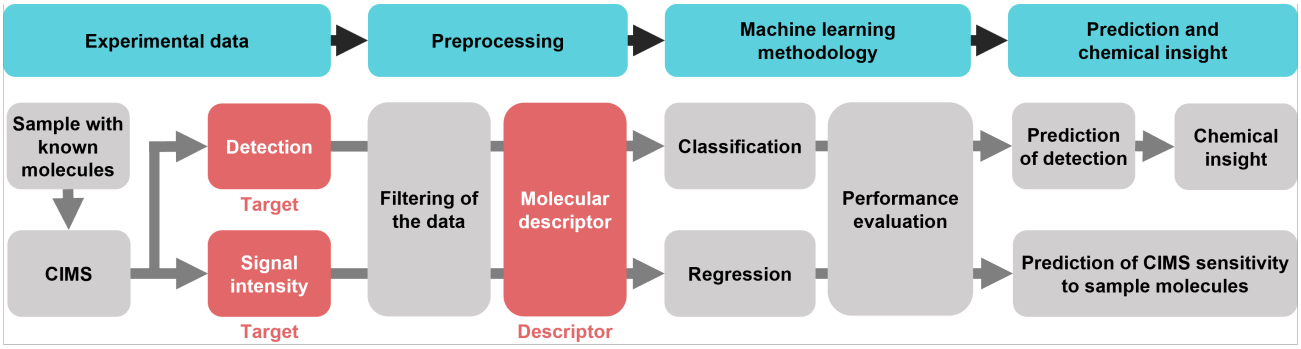

Figure 1. Schematic of the machine learning workflow followed in this work: the sample is analyzed and the two targets of our analyses are defined; the preprocessing includes the filtering of the data and the creation of the molecular descriptors which will be fed into the ML algorithms; the two ML models are divided into classification (to predict whether a molecule is detected or not) and regression (to predict the CIMS sensitivity of a molecule); the performances of the models are evaluated and chemical insight is extracted from the feature analysis.

2 Dataset

Our dataset is generated from two standard mixtures purchased from GALAB Laboratories, containing 404 and 312 organic pesticides. The CIMS experiments were conducted at Karsa Oy laboratory (Karsa) with a TD-MION inlet operating at atmospheric pressure coupled to a linear trap quadrupole orbitrap mass spectrometer. A schematic of the instrument is presented in Partovi et al. (2023, 2024b). The mixtures were individually measured at five different concentrations, but for this work, only measurements at the highest concentration (2,5 ng μl^{-1}) were considered. The measurements from the two mixtures were combined into a single dataset for a total of 716 pesticide observations. Each pesticide was measured with the following ionization schemes: bromide (Br^-) ionization (produced from dibromomethane, CH_2Br_2); protonated acetone ($(CH_3)_2COH^+$, $AceH^+$) ionization (produced from acetone, $(CH_3)_2CO$); proton-transfer (H^+) ionization by hydronium ions (H_3O^+, produced

https://doi.org/10.5194/egusphere-2024-1846
Preprint. Discussion started: 18 July 2024

from trace amounts of water, H_2O^+); and electron transfer (-) ionization by dioxide (O_2^-). The two latter ions were obtained by feeding dopant-free air into the ion source.

From the 716 measured pesticides, we removed 23 from the dataset (Fig. S3, Table S1 and Table S2 in the Supplementary Information, SI) for the following reasons. Twelve instances correspond to six pesticides that appeared twice (once in each mixture) but were measured with different signal intensities. Next, we excluded 10 pesticides with a molecular weight outside the ideal mass spectrometer transmission window, i.e., lower than 120 u and higher than 600 u, which suffered from the corresponding significant signal loss. Another pesticide was excluded due to its out-of-range Br^- intensity value. As a side note, several isomers (e.g. prometryn and terbutryn, or phoxim and quinalphos) are present in the dataset. In CIMS, isomers produce peaks at the same mass-to-charge ratio and cannot be distinguished with a single ionization method, as they can in, e.g., fragmentation mass spectrometry. We decided to keep all isomers to not reduce our data set volume further, but we are aware that this decision introduces additional uncertainty in the dataset. In the following, *dataset* refers to the 693 pesticides remaining after removing the aforementioned 23 pesticides.

Figure 2 presents basic dataset statistics (molecular size, element composition and detection by ionization method). In Panel (a) and (b), we distinguish between *detected* and *undetected*. If the signal intensity of a molecule is zero for all ionization methods, it is considered undetected and detected otherwise. In panel (c), we make the same distinction but for each ionization method individually. The number of non-hydrogen atoms per molecule (Figure 2a) is normally distributed for detected and undetected pesticides with an average of 20 atoms per pesticide (dashed vertical line). The smallest molecule, methamidophos, contains 7 atoms, while the largest one, acrinathrin, contains 38 atoms. In total, we find 572 pesticides, for which at least one ionization method gives a signal, and 121 undetected pesticides, for which no ionization method triggers.

https://doi.org/10.5194/egusphere-2024-1846
Preprint. Discussion started: 18 July 2024

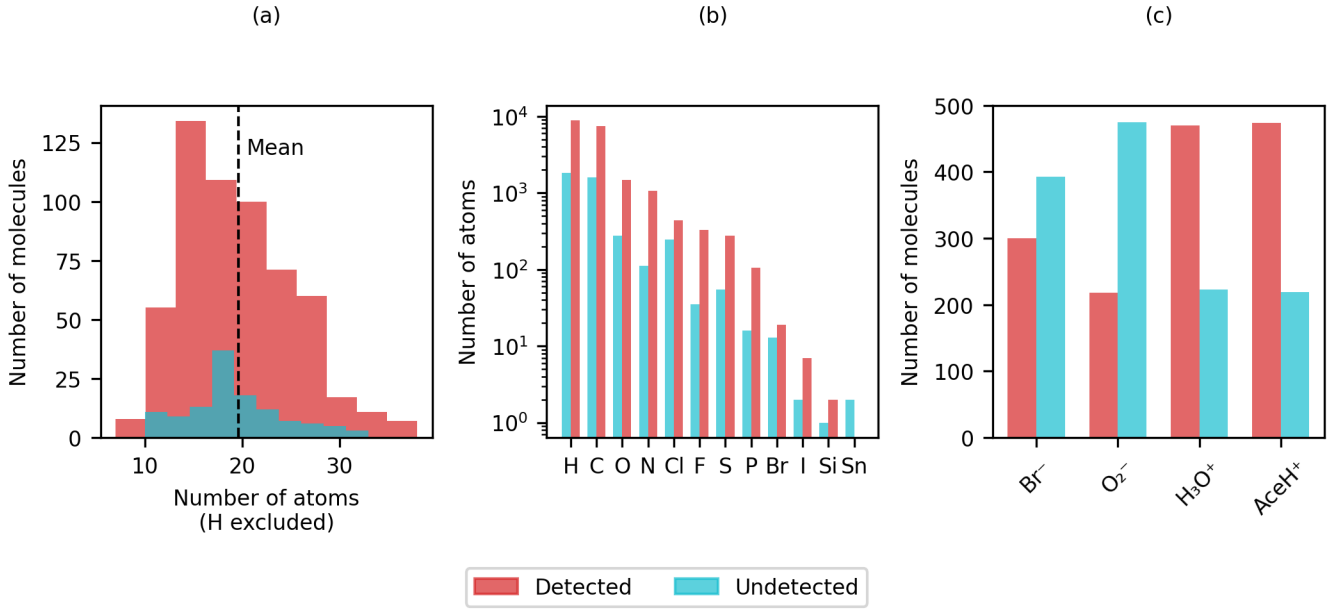

Figure 2. Distribution of (a) heavy atoms, (b) element types in logarithmic scale and (c) detection rate of the four reagent ions (Br^-, O_2^-, H_3O^+ and $AceH^+$). The legend presents the number of detected pesticides in red and undetected pesticides in light blue. In Panel (a) and (b), a pesticide is part of the detected count when at least one ionization method presents a signal. In Panel (c) the pesticides are counted as detected and undetected based on the signal intensity value of each ionization method individually.

Figure 2b shows a histogram of the chemical elements present in the dataset. The pesticides in our dataset are organic molecules and therefore have a prevalence for hydrogen, carbon, nitrogen and oxygen. In addition, chlorine, fluorine, sulfur, and phosphorus, are present in over a hundred pesticides, whereas bromine, iodine, silicon and tin occur less frequently. Tin is the only element present only in undetected molecules (Table S3 in the SI presents a list of tin compounds).

In Figure 2c the total count of detected and undetected pesticides for each ionization method is shown. In contrast to the positive reagent ions, the two negative reagent ions exhibit a higher number of undetected molecules than detected ones. Most pesticides are detected with $AceH^+$ and fewest with O_2^-. The figure highlights that negative reagent ions are more selective than positive ones.

Table 1 presents six examples of chemical diversity in our dataset. The first two entries correspond to the smallest and the largest pesticides (methamidophos (7 atoms) and acrinathrin (38 atoms)). Subsequent entries highlight the diversity in functional groups. The molecular complexity ranges from 1-naphthaleneacetic acid (containing naphthalene with acetic acid substituent) to trichlorfon (containing oxygen, nitrogen, fluorine, sulfur and aromatic rings), alpha-HCH (cyclohexane with 6 chlorine substituents) or tritosulfuron (containing 3 chlorine, 4 oxygens and a phosphorus atom over 12 total atoms).

https://doi.org/10.5194/egusphere-2024-1846
Preprint. Discussion started: 18 July 2024

Table 1. Example of the chemical diversity of the dataset.

Name	Number of atoms	Molecular weight [u]	Detected with:	Structure
Methamidophos	7	141.00	H_3O^+; $AceH^+$	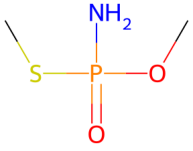
Acrinathrin	38	541.13	Br^-; O_2^-; $AceH^+$	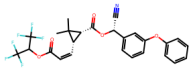
1-Naphthaleneacetic acid	14	186.07	O_2^-; $AceH^+$	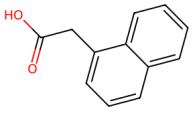
Tritosulfuron	29	445.03	O_2^-	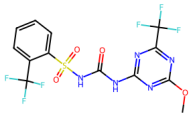
alpha-HCH	12	287.86	Br^-; O_2^-	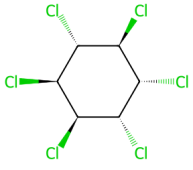
Trichlorfon	12	255.92	Br^-; H_3O^+; $AceH^+$	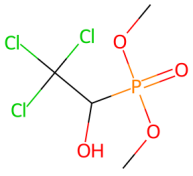

Figure 3 presents the logarithmic signal intensity distribution (panel a) and the scatter matrix of the logarithmic signal intensity (panel b) for each reagent ion. In panel a, both $AceH^+$ and H_3O^+ are normally distributed. The distribution for O_2^-

https://doi.org/10.5194/egusphere-2024-1846
Preprint. Discussion started: 18 July 2024

is flatter (probably due to the small number of detected molecules) and Br^- is almost homogeneously distributed across the intensity range. Panel b visualizes the bivariate relationship between (logarithmic signal intensities) for the pesticides detected with all four reagent ions. Only the two positive ionization schemes $AceH^+$ and H_3O^+ exhibit a clear correlation (R^2=0.6). The negative ionization schemes O_2^- and Br^- are not as well correlated (R^2=0.2). Meanwhile, the inter-correlation between positive and negative reagent ions is below 0.07. The general lack of correlation between ionization schemes indicates that different reagent-ions probe different parts of the target molecules.

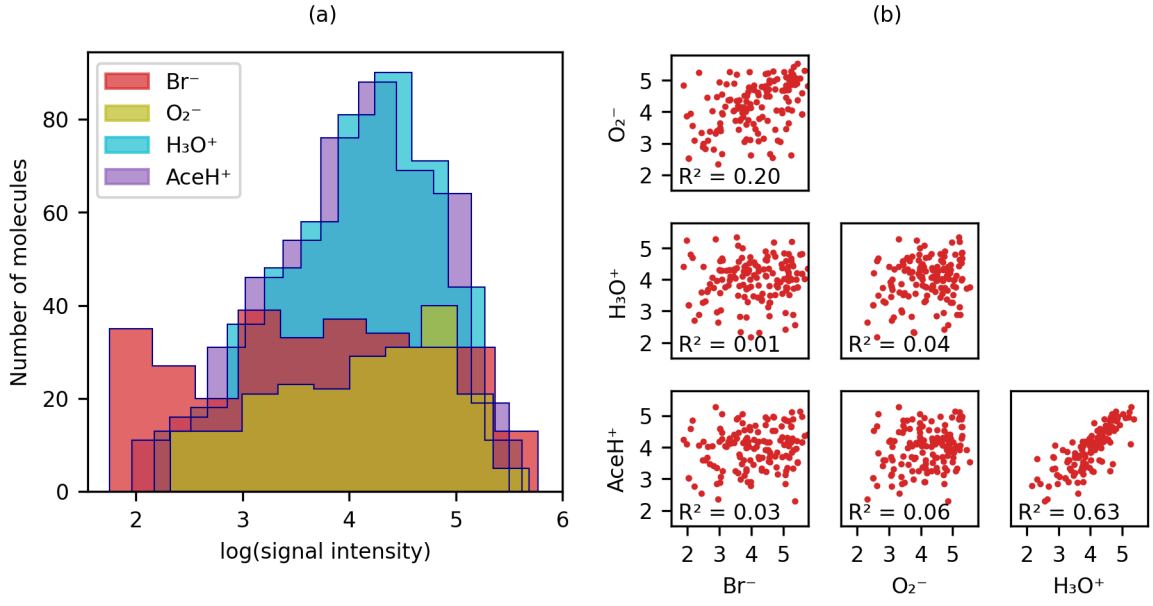

Figure 3. (a) Detected molecules signal intensity distribution shown on a logarithmic scale for the four reagent ions and (b) scatter matrix for the four reagent ions.

Figure 4 shows the t-stochastic neighbourhood embedding (t-SNE) of the logarithmic signal intensity values. t-SNE (van der Maaten and Hinton, 2008) visualizes high-dimensional data in lower dimensions preserving the similarity of data points. We used the *scikit-learn* implementation of t-SNE (*sklearn.manifold.TSNE*, Pedregosa et al. (2011)) with a random state of 42, a perplexity of 50 and a maximum number of iterations of 5000. We then assigned different colours and symbols to the ionization method combinations that detected a given pesticide.

Clear clusters of the same colour and the same symbol emerge in the t-SNE plot in Figure 4. Only one cluster is composed of molecules detected with both Br^- and $AceH^+$ (yellow squares), Br^- and H_3O^+ (yellow circles), and Br^-, $AceH^+$ and H_3O^+ (blue squares). From this we conclude, that Br^- delivers the most information for these pesticides and the positive ionization method is of lesser importance. The situation is similar for H_3O^+ and $AceH^+$ that appear in two clusters where blue triangles (H_3O^+, $AceH^+$, Br^-) come close to yellow crosses (H_3O^+, O_2^-) and blue stars ($AceH^+$, Br^-, O_2^-) close to yellow diamonds

https://doi.org/10.5194/egusphere-2024-1846
Preprint. Discussion started: 18 July 2024

(AceH$^+$, Br$^-$) and squares (AceH$^+$, O_2^-). The presence of clear clusters suggests that the CIMS signals carry information that might allow ML to distinguish different pesticides.

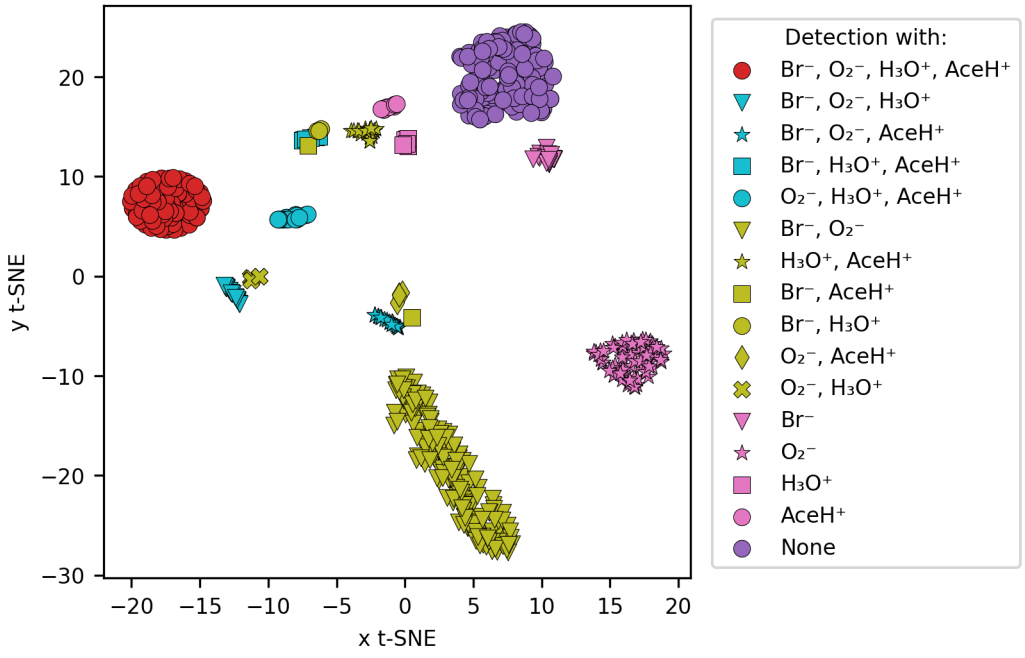

Figure 4. Similarity between the signal intensity of the molecules by using t-SNE clustering. The comparison was based on the logarithmic signal intensity and each cluster follows a color-code based on the detection type (all the possible combinations between the four reagent ions).

3 Molecular descriptors

Molecular representations transform molecular structures into readable input for ML methods. These descriptors are numerical representations of atomistic systems that should fulfil certain requirements, such as being invariant to spatial and rotational transformations, invariant to permutation of atomic indices, unique, continuous, compact and computationally efficient (Himanen et al., 2020; Huo and Rupp, 2022; Rupp, 2015; Xue and J, 2020; Langer et al., 2022). However, a universal descriptor able to perform well for every chemical system and task does not exist. For this reason, we tested five different descriptors (Fig. 1a) for our classification and regression tasks. We investigated a property-based descriptor (RDKitPROP), two structure-based descriptors (TopFP and MACCS) derived from SMILES (Simplified Molecular-Input Line-Entry System) strings, and two structure-based descriptors obtained from the Cartesian coordinates of the atoms in the molecules (CM and MBTR) (Landrum, 2006; Durant et al., 2002; Rupp et al., 2012; Huo and Rupp, 2022). The Cartesian coordinates were obtained from the SMILES string of each pesticide through geometry optimization with a universal force field implemented in *RDKit* (Landrum, 2006). Figure 5 depicts visual examples of four descriptors. The representations are discussed in more detail in the following sections.

https://doi.org/10.5194/egusphere-2024-1846
Preprint. Discussion started: 18 July 2024

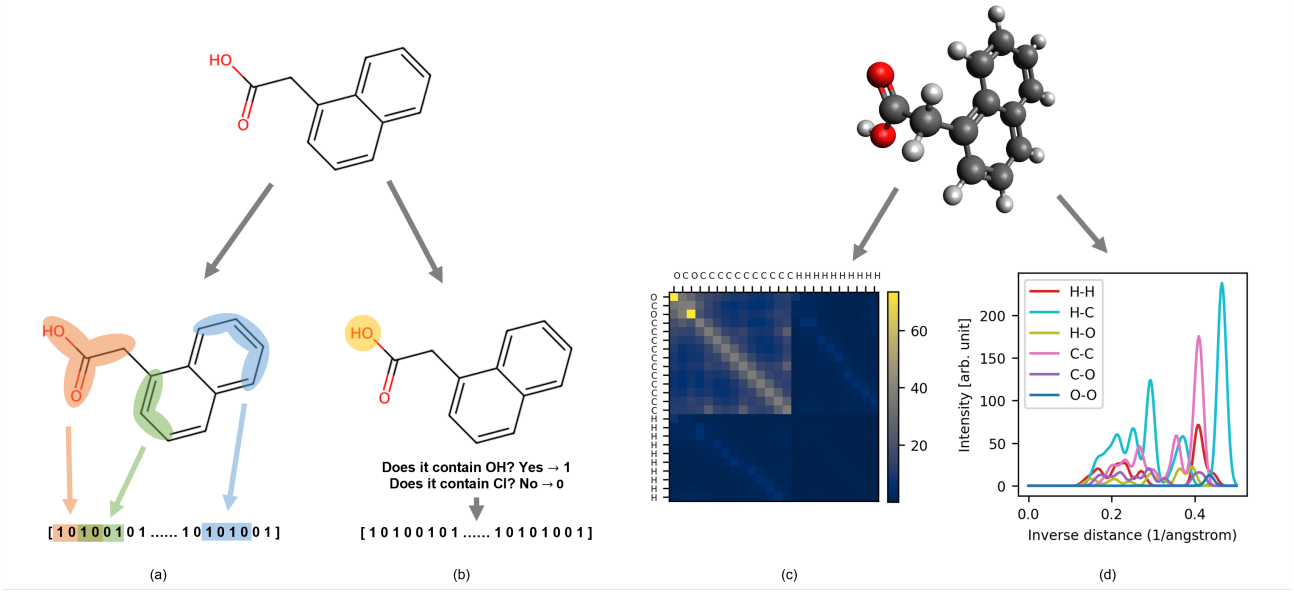

Figure 5. Visual example of 1-Naphthaleneacetic acid molecular representations: on the left descriptors computed from SMILES, (a) topological fingerprint (TopFP), (b) molecular access system keys (MACCS); on the right descriptors computed from XYZ coordinates, (c) coulomb matrix (CM), (d) many-body tensor representation (MBTR).

3.1 Property-based descriptor (RDKitPROP)

RDKitPROP includes 43 properties computed from the molecular structure of the pesticides (represented by a SMILES string), by applying the function *rdkit.Chem.rdMolDescriptors.Properties* (Landrum, 2006). In the SI, we describe these properties in more detail (Table S4). In Sect. 5, we will discuss only a subset of the five most important properties for the best classifier (see Sect. 4.1). These properties are the topological polar surface area (TPSA, (Ertl et al., 2000)), the number of hydrogen bond donors (HBD), the number of hydrogen bond acceptors (HBA), the Wildman-Crippen logarithm of the partition coefficient (CrippenClogP, (Wildman and Crippen, 1999)), the fraction of sp^3 carbons (FractionCSP3), the Hall-Kier alpha value (HallKierAlpha, (Hall and Kier, 1991)) and the molecular weight. TPSA calculates the polar surface area by summing the contribution of individual fragments containing nitrogen, oxygen, phosphorus and sulfur. The HallKierAlpha value is the sum of the scaled measures of each atom's covalent radius, adjusted for its hybridization state and electronegativity. The scaling is relative to the covalent radius of a sp^3 hybridized carbon atom. CrippenClogP measures the hydrophobicity of a molecule while the FractionCSP3 indicates the saturation of carbon atoms in the molecule. The number of HBA counts the oxygen and nitrogen atoms in the molecule. In the descriptor, two distinct properties address this value (LipinskiHBA and NumHBA). The number of HBD calculates the number of hydrogen atoms attached to oxygen and nitrogen atoms in the molecule (addressed by LipinskiHBD and NumHBD). Lastly, the molecular weight is addressed as well by two distinct properties: the average molecular weight (AMw) and the exact molecular weight (ExactMw).

https://doi.org/10.5194/egusphere-2024-1846
Preprint. Discussion started: 18 July 2024

3.2 Topological fingerprint (TopFP)

TopFP (Fig. 5a) implemented in RDKit (Landrum, 2006) is a molecular descriptor inspired by the Daylight fingerprint (James et al., 1995). This fingerprint extracts molecular fragments of a certain size by starting from one atom and following the bond topology. A mathematical function converts each fragment into a bit string (hashing) and all strings are concatenated into the final fingerprint. In the implementation, the length of the path, the number of bits per hash and the final size of the fingerprint are called hyperparameters and can be optimized to improve the performance of the descriptor. TopFP is easily implemented at a reasonable computational cost. However, the hash function makes interpretation difficult as there is no one-to-one correspondence between fragments and bits.

3.3 Molecular access system keys (MACCS)

MACCS also encodes molecular features as binary string (Durant et al., 2002) (Fig. 5b). Unlike TopFP, however, bits correspond to the one-hot encoding of specific predefined questions, such as 'Does the molecule contain a carbonyl group?' (Yes: 1, No: 0). In this work we used the *RDKit* MACCS implementation, which encompasses a total of 166 keys (Landrum, 2006), making this descriptor fast to run. However, MACCS is limited in the number of implemented questions and any structural or chemical information not captured by these questions is lost.

3.4 Coulomb matrix (CM)

The Coulomb matrix (Fig. 5c) encodes both the cartesian coordinates and the nuclear charges of each atom in the molecule as a $n \times n$ matrix, where n is the number of atoms in the molecule:

$$M_{IJ} = \begin{cases} 0.5 Z_I^{2.4} & \forall\, I = J \\ \frac{Z_I Z_J}{|R_I - R_J|} & \forall\, I \neq J. \end{cases} \tag{1}$$

Z_I is the atomic number of atom I and $|R_I - R_J|$ the Euclidean distance between the atoms I and J. The elements on the diagonal were fitted to atomic energies, while the off-diagonal elements encode a Coulomb repulsion between each atom pair in the molecule (Rupp et al., 2012). Compared to other three-dimensional representations, the CM is straightforward to interpret, easy to implement, and fast to compute. This simplicity, however, comes with a loss of detail, e.g. bond connectivity, which may be relevant for larger molecules such as pesticides.

In this work, we used the DScribe (Himanen et al., 2020) implementation of the CM. The CM has no hyperparameters to optimize, which adds to its appeal.

3.5 Many-body tensor representation (MBTR)

The MBTR (f_K, Fig. 5d) captures the 3D structure of a molecule in a continuous way (Huo and Rupp, 2022):

https://doi.org/10.5194/egusphere-2024-1846
Preprint. Discussion started: 18 July 2024

$$f_K(x) = \frac{1}{\sigma_K\sqrt{2\pi}} e^{-\frac{(x-g_K(K))^2}{2\sigma_K^2}}. \quad (2)$$

Here σ_K is the standard deviation of the Gaussian kernel, g_K a geometry function with input K for many-body rank k. The first term ($k = 1$) encodes only elemental features ($K = Z_i$). The second term ($k = 2$) records inverse or direct distances between atoms $K = \frac{1}{|R_i - R_m|}$ or $K = |R_i - R_m|$ and the third term ($k = 3$) angles between three atoms $K = \angle(R_i - R_m, R_n - R_m)$ (or $K = \cos(R_i - R_m, R_n - R_m)$). Because the three terms are tabulated on a grid, this descriptor is the largest one we tested.

In this work, we used the DScribe (Himanen et al., 2020; Laakso et al., 2023) implementation of the MBTR. We used only the $k = 2$ and $k = 3$ terms, since including the first term did not improve the performance but increased the computation time (see Fig. S6 in the SI). We used inverse distances and the cosine for K=2 and K=3, respectively, and applied exponential weighting to determine the relative importance of each term. The tuned hyperparameters are the Gaussian broadening parameter σ_2 and σ_3 and the scale of the weighting referred to as w_2 and w_3 (Himanen et al., 2020).

4 Machine learning methods

In this section, we briefly introduce the two ML methods that we use in this work. To classify, if a pesticide is detectable or not with a specific ionization method, we will train a RF classifier. Subsequently, we will investigate, if we can predict the corresponding CIMS intensity with KRR.

4.1 Random forest classifier (RF)

RF (Breiman, 2001) is a ML method that combines different decision trees, each of which learns the relation between input and output features in terms of simple decision rules. Each tree is trained on a subset of the data and input features. Additional bootstrapping decreases the variance of the prediction by resampling the training set observations. In this work, we used a *scikit-learn* RF classifier (*sklearn.ensemble.RandomForestClassifier*). Each tree gives a class probability prediction (detected or undetected) and the final prediction is an average of the probability given by each tree. We optimized the following hyperparameters: the maximum number of estimators (the trees creating the forest), the maximum depth of each tree (the length from the starting point, "root", to the final points, "leaves"); the minimum number of samples per leaf, to ensure that each leaf has an adequate number of data points to avoid overfitting and underfitting; the minimum number of sample splits, to ensure that each internal node (which can branch again) has an adequate number of samples.

4.2 Kernel Ridge Regression (KRR)

Regression is a statistical process that determines the strength and character of the relationship between one dependent variable and a series of other variables. In this work, we perform kernel ridge regression (KRR) to include non-linearities (kernel) and

https://doi.org/10.5194/egusphere-2024-1846
Preprint. Discussion started: 18 July 2024

prevent over-fitting (ridge regression (Hoerl and Kennard, 1970)). The kernel model (f) is expressed as a linear sum over kernel functions k over the training samples x_i

$$f(\widetilde{x}) = \sum_{i=1}^{n} \alpha_i k(x_i, \widetilde{x}). \tag{3}$$

The expansion coefficients α_i follow from the minimization of the ridge loss function

$$\arg\min_{\alpha \in \mathbb{R}^n} \sum_{i=1}^{n} (f(x_i) - y_i)^2 + \lambda \|f\|_H^2 \quad \rightarrow \quad \alpha = (K + \lambda I)^{-1} y. \tag{4}$$

Here K is the kernel matrix, I is the identity matrix and $\|f\|_H$ is the norm of f in the feature space. We use the Gaussian kernel

$$k(\mathbf{x}_i, \mathbf{x}_j) = \exp\left(-\frac{\|\mathbf{x}_i - \mathbf{x}_j\|_2^2}{2\sigma^2}\right) \tag{5}$$

where σ is the length scale hyperparameter. In this work, we applied the KRR implementation (*sklearn.kernel_ridge.KernelRidge*) from *scikit-learn*.

4.3 Performance metrics

The classification performance will be tested by calculating the accuracy of the class prediction. The accuracy score is the fraction of correct predictions compared to the total number of observations present in a test set:

$$\text{accuracy}(y, \hat{y}) = \frac{1}{n} \sum_{i=0}^{n-1} 1(\hat{y}_i = y_i) \tag{6}$$

where $\hat{y}_i$ is the i-th predicted class, y_i is its reference class and n the number of samples in the test set.

The receiver operating characteristic (ROC) curve provides us with an additional performance assessment. The curve puts the correctly classified pesticides (true positive rate, vertical axis) in relation to the incorrectly classified ones (false positive rate, horizontal axis), across a range of different threshold levels. The area under the curve (AUC) quantifies the overall ability of the classifier to distinguish between the detected class and the undetected class (Géron, 2022). The more the curve shifts towards the top-left corner (with an AUC corresponding to 1), the better the classification. A random classifier would correspond to a diagonal line with an AUC of 0.5.

The regression performance will be assessed with the mean absolute error (MAE), a metric commonly used to measure the average absolute difference between a variable's predicted and reference values. Unlike other metrics, MAE does not penalize outliers as it assigns equal weight to all errors (Rupp, 2015). The MAE is defined as

$$\text{MAE}(y, \hat{y}) = \frac{1}{n} \sum_{i=0}^{n-1} |y_i - \hat{y}_i|, \tag{7}$$

https://doi.org/10.5194/egusphere-2024-1846
Preprint. Discussion started: 18 July 2024

where $\hat{y}_i$ is the predicted value of the i-th sample, y_i is the corresponding true value in the dataset and n is the number of observations.

4.4 Computational details

We train a separate classification and regression model for each ionization method. The datasets were randomly split into test (20%) and training (80%) sets. The training set is further split into six subsets to create a learning curve. Each model was trained with five different random splits (i.e., different random seeds) to average out data variability and to collect statistics. Additionally, we optimized the hyperparameters with 5-fold cross-validation using random search implemented by *scikit-learn* (*sklearn.model_selection.RandomizedSearchCV*), which is efficient in higher dimensions (Stuke et al., 2021).

We trained binary classifiers that distinguish only between two classes (class 1: detected, class 0: undetected), for which we have a maximum of 554 training points (80% of the data). The regressors were trained on the logarithmic CIMS intensity of the detected pesticides. This gives us a maximum of 240 data points for Br^-, 174 for $O_2{}^-$, 376 for H_3O^+, and 379 for $AceH^+$.

In Sect. S4 of the SI, we provide the optimized hyperparameters for each model and each random seed. Tables S6, S7, S8, S9, and S10 report the RF hyperparameters and Tables S11, S12, S13, S14, and S15 the KRR hyperparameters for each molecular descriptor.

5 Results and discussion

5.1 CIMS detection prediction

The classification ROC curves and relative AUC values for each ionization scheme are presented in Fig. 6 for the five molecular descriptors. All ROC curves lie above the diagonal, which implies that our RF models can classify if a pesticide is detectable based on its atomic and chemical structure. However, they do so with varying degrees of success. The best performance is achieved with the MACCS, MBTR and RDKitPROP descriptors, with average AUC values above 0.86. The TopFP and CM descriptors perform worse, in particular for the negative ionization schemes, most likely due to the smaller number of training samples.

https://doi.org/10.5194/egusphere-2024-1846
Preprint. Discussion started: 18 July 2024

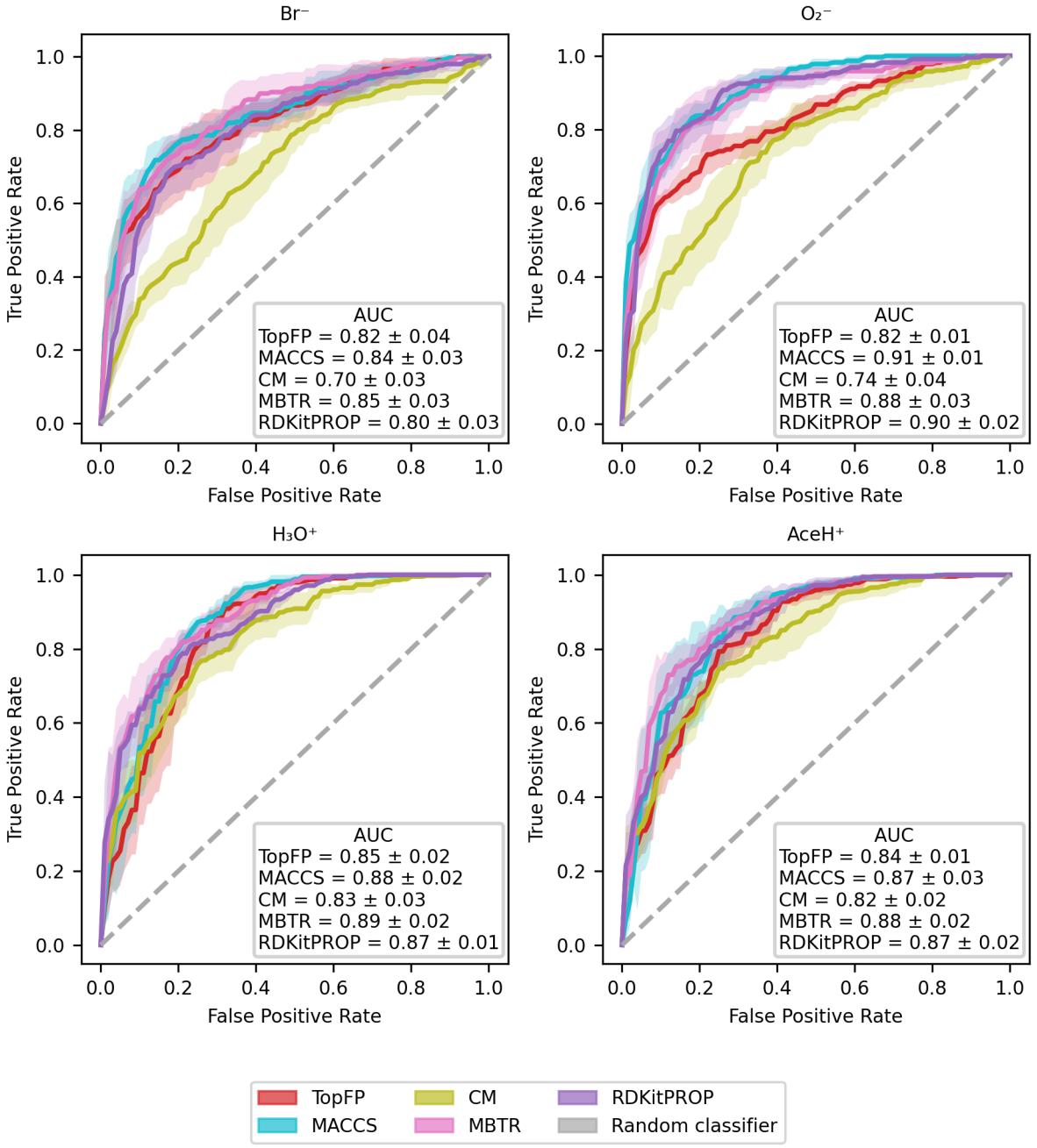

Figure 6. Evaluation of the classification performance with RF, by the use of ROC curves for the four ionization schemes (Br^-, O_2^-, H_3O^+, $AceH^+$) with the five molecular descriptors (MACCS, MBTR, TopFP, CM, properties). For each curve, we report the AUC value. The x-axis reports the false positive rate, the y-axis reports the true positive rate. The mean value and standard deviation are obtained by repeating the training with five different random re-shuffling of the dataset.

https://doi.org/10.5194/egusphere-2024-1846
Preprint. Discussion started: 18 July 2024

Table 2 reports the classification accuracy for each reagent ion over five random re-shuffles of the datasets. The learning curves for the accuracy can be found in the SI (Fig. S7), where we also present the learning curves for similar performance metrics such as recall, precision and F1 score (Fig. S8, Fig. S9 and Fig. S10, respectively). All classification models reach an accuracy above 0.6. The CM descriptor shows the worst overall performance for Br^- (0.64 ± 0.04 of accuracy) and MACCS reaches the best overall performance for H_3O^+ (0.85 ± 0.02 of accuracy). In general, the accuracy is lost for Br^-, while $O_2{}^-$ is en par with H_3O^+ and $AceH^+$. Overall, MBTR and MACCS yield the highest accuracy, followed by TopFP and RDKitPROP and then CM.

Table 2. Accuracy Mean value and standard deviation of the prediction on the test dataset with RF for all reagent ions with the five different molecular descriptors. The values were obtained by repeating the training on the largest training size (80% of the dataset) with 5 different random re-shuffling of the dataset.

Ionization method	Training size	Descriptor	Accuracy
Br^-	554	TopFP	0.75 ± 0.04
		MACCS	0.78 ± 0.02
		CM	0.64 ± 0.04
		MBTR	0.76 ± 0.06
		RDKitPROP	0.76 ± 0.03
$O_2{}^-$	554	TopFP	0.78 ± 0.06
		MACCS	0.83 ± 0.04
		CM	0.73 ± 0.05
		MBTR	0.80 ± 0.04
		RDKitPROP	0.84 ± 0.02
H_3O^+	554	TopFP	0.83 ± 0.02
		MACCS	0.85 ± 0.02
		CM	0.76 ± 0.02
		MBTR	0.81 ± 0.01
		RDKitPROP	0.79 ± 0.03
$AceH^+$	554	TopFP	0.80 ± 0.02
		MACCS	0.83 ± 0.02
		CM	0.76 ± 0.03
		MBTR	0.82 ± 0.01
		RDKitPROP	0.83 ± 0.02

https://doi.org/10.5194/egusphere-2024-1846
Preprint. Discussion started: 18 July 2024

MBTR is the largest and most complex descriptor we have tested. Its good performance is similar to previous observations for vapour pressure (Lumiaro et al., 2021) and ionization energy predictions (Stuke et al., 2019). The fact that the MACCS key achieves a similar performance is at first surprising because it performed poorly in the earlier studies. The good classification performance reported here, however, indicates that the chemical complexity of the pesticides is well captured by the questions encoded in the MACCS key.

The ROC curves and the accuracy metrics demonstrate good discriminative capabilities for predicting pesticide detection. This performance is particularly noteworthy given the challenges posed by the class imbalance in the dataset and the relatively small training set of just 554 observations, which is modest compared to typical ML applications. The fact that all models classify well indicates that they can capture the inherent chemical and structural diversity of the pesticides, which can provide additional insight into the interaction between the target molecules and reagent ions (see Sect. 5.3).

With an accuracy and AUC of around 0.8 our best-performing models are good enough to be useful in deployments. We expect that the trained models can predict detection with CIMS (specifically with Br^-, $O_2{}^-$, H_3O^+, or $AceH^+$ as reagent ions) for molecules with similar structural features to those in our dataset. This could speed up laboratory analyses or field deployment for measuring campaigns or safety and security systems since one can *a priori* check if a pesticide will be detectable without having to perform a CIMS experiment.

5.2 Quantitative prediction of CIMS sensitivity to target molecules

We now turn to evaluate the performance of the regression models tasked to predict the CIMS sensitivity of the pesticides. The MAE learning curves of the KRR models are shown in Fig. 7 for five random seeds and the different descriptors. For all the reagent ions, the MAE decreases with increasing training size indicating that our models indeed learn with data. The learning rate is comparable to earlier work Lumiaro et al. (2021); Stuke et al. (2019) that used much larger datasets. Usually, the variance decreases with increasing dataset size, which is not the case in Fig. 7. We ascribe that the variance across the learning curves is moreless similar to the fact that our datasets are extremely small.

https://doi.org/10.5194/egusphere-2024-1846
Preprint. Discussion started: 18 July 2024

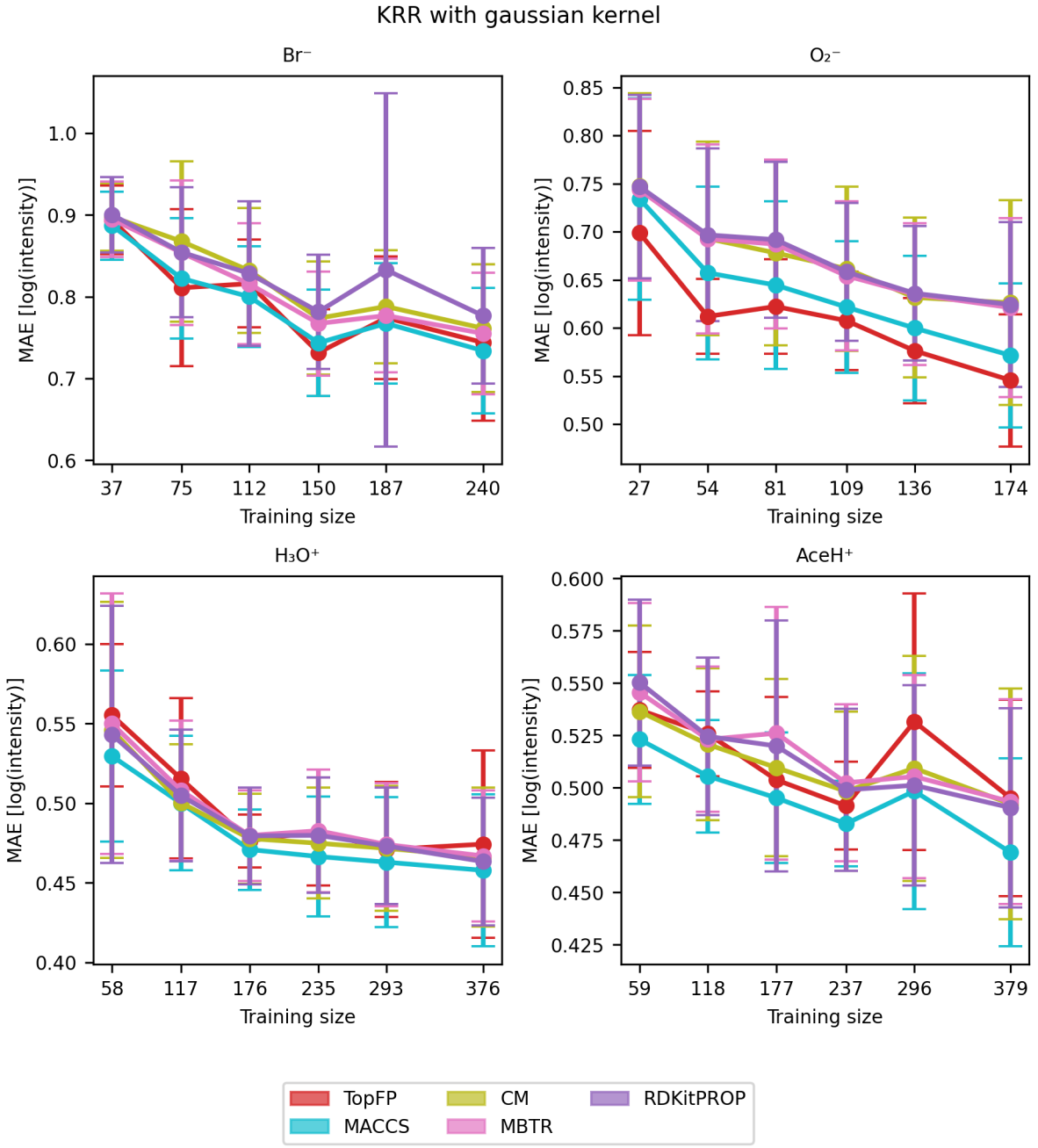

Figure 7. Learning curve with mean absolute error (MAE) of the signal intensity values in logarithmic scale of Br^-, O_2^-, H_3O^+ and $AceH^+$ datasets, based on the TopFP, MACCS, CM, MBTR and properties as the descriptors. The x-axis reports the training set size, the y-axis reports the MAE of the logarithmic signal intensity. The mean value and standard deviation are obtained by repeating the training with five different random re-shuffling of the dataset.

https://doi.org/10.5194/egusphere-2024-1846
Preprint. Discussion started: 18 July 2024

Table 3 presents the average MAE values for the highest training size for each ionization method and descriptor averaged over the five random seeds. All trained models achieved an error lower than one logarithmic unit of signal intensity. Such low MAEs present a significant achievement considering both the complex task and the small size of the dataset and the fact that CIMS signals vary over several orders of magnitude.

We find the lowest MAEs for the positive ionization methods, most likely, because the available datasets are larger. Unlike for classification, the different descriptors perform similarly for the regression task. Overall, MACCS is still the best, followed by TopFP and the MBTR. The fact all descriptors learn similarly is surprising since they capture different features of the elemental and structural features. We attribute this behaviour to the fact that the CIMS intensity correlates with the binding strength of the reagent ion (Partovi et al., 2023; Iyer et al., 2016; Hyttinen et al., 2018), but none of the descriptors took the reagent ion into account. We suspect that refined descriptors that target the combined ion-molecule ensemble will perform better.

https://doi.org/10.5194/egusphere-2024-1846
Preprint. Discussion started: 18 July 2024

Table 3. Mean absolute errors (MAE) and standard deviation of the prediction on the test dataset with KRR for all reagent ions with the five different molecular descriptors. The values were obtained by repeating the training on the largest training size (80% of the detected dataset) with 5 different random re-shuffling of the dataset.

Ionization method	Training size	Descriptor	MAE [log(signal intensity)]
Br^-	240	TopFP	0.74 ± 0.10
		MACCS	0.72 ± 0.06
		CM	0.82 ± 0.05
		MBTR	0.74 ± 0.07
		RDKitPROP	0.86 ± 0.06
$O_2{}^-$	174	TopFP	0.55 ± 0.07
		MACCS	0.60 ± 0.08
		CM	0.74 ± 0.07
		MBTR	0.61 ± 0.03
		RDKitPROP	0.64 ± 0.05
H_3O^+	376	TopFP	0.47 ± 0.06
		MACCS	0.44 ± 0.03
		CM	0.48 ± 0.03
		MBTR	0.47 ± 0.04
		RDKitPROP	0.45 ± 0.04
$AceH^+$	379	TopFP	0.50 ± 0.05
		MACCS	0.44 ± 0.03
		CM	0.54 ± 0.05
		MBTR	0.50 ± 0.03
		RDKitPROP	0.48 ± 0.04

The results demonstrate that all models can achieve a MAE under one unit of logarithmic signal intensity, which is impressive, especially considering the even lower number of observations compared to the classification task (174 in the worst case). Such an accuracy is already sufficient for deployment in field studies. For suspected molecules or pollutants, ML models could estimate the expected signal intensity, and subsequently its concentration in the atmosphere without relying on quantum chemical computations or direct measurements. Conversely, insight into the detection processes could be garnered by identifying chemical features that correlate with the signal intensity for the different ionization methods. We will present such analysis in the next section.

https://doi.org/10.5194/egusphere-2024-1846
Preprint. Discussion started: 18 July 2024

5.3 Chemical insight

Next, we will extract chemical insight from our ML models. RF provides access to the feature importance, i.e., to the input features that correlate most strongly with the output. This feature importance provides insight into the complex ion-molecule interactions. We will focus on the MACCS and RDKitPROP descriptors because they are the most interpretable. For each ionization method, we pick the largest training set size and then obtain the feature ranking and the corresponding coefficients (importance values) from the trained RF models for the five random seeds. We then average the importance values for each feature and rank again.

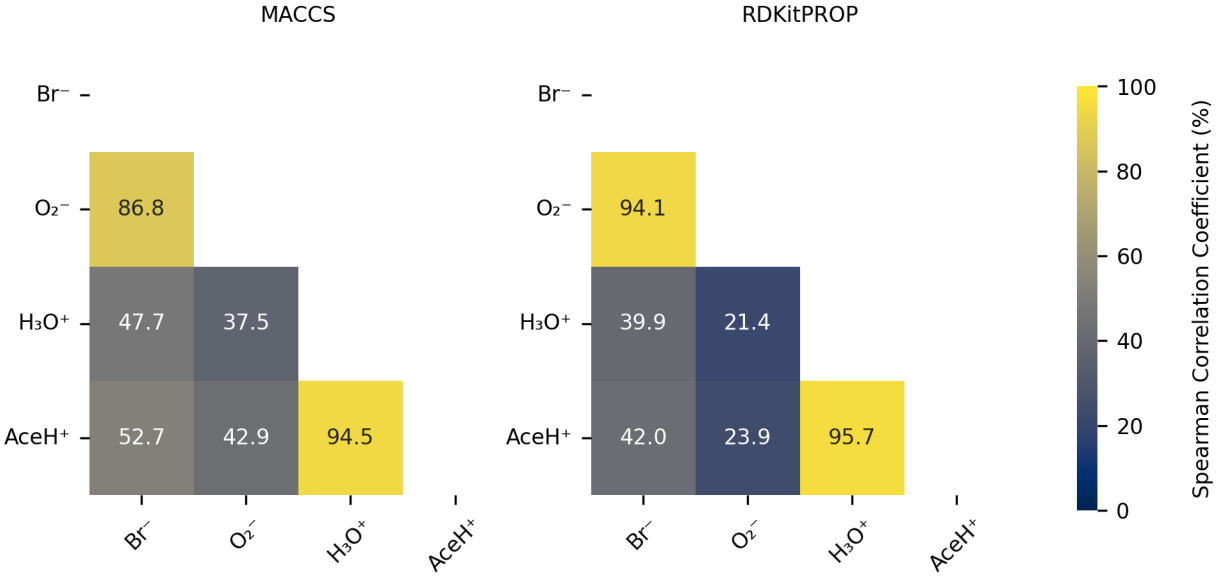

Figure 8. Pearson correlation coefficient (%) of the normalized features importance values obtained from the RF estimator trained on 80% of the data with optimized hyperparameters based on MACCS and RDKitPROP.

We then compare the most important features of a given ionization method to those of the other ionization methods by means of the Pearson correlation coefficient. Figure 8 shows the Pearson correlation coefficient of the normalized feature importance values in percentage for the RDKitPROP and MACCS descriptors. For both descriptors, the features for the negative (Br^- and $O_2{}^-$) and positive ionization methods (H_3O^+ and $AceH^+$) correlate strongly (above 86.8%). The inter-correlation between the features of the positive and negative reagent ions, however, is much weaker (between 21.4% and 52.7%). The Pearson correlation coefficients reveal that the polarity of the reagent ion predominately determines which molecular features the ion interacts with. We made a similar observation in Fig. 3b, where we saw that the signal intensities cluster strongly by the polarity of the reagent ion.

Figure 9 reports the importance values in percentage for the most important features of the RDKitPROP model for the four ionization methods. Table S16 and Table S17 in the SI provide the values for all the properties, and additionally, the

https://doi.org/10.5194/egusphere-2024-1846
Preprint. Discussion started: 18 July 2024

average value of the property calculated individually for detected and undetected pesticides. No feature has an importance above 10% and only four of them reach an importance above 6 %: TPSA, LipinskiHBA in the case of positive reagent ions, and LipinskiHBD and NumHBD in the case of negative reagent ions. The next most important properties are NumHBA and NumAtoms for positive ionization methods and then HallKierAlpha, CrippenClogP, FractionCSP3, AMw and ExactMw presenting similar importance for both positive and negative ionization methods.

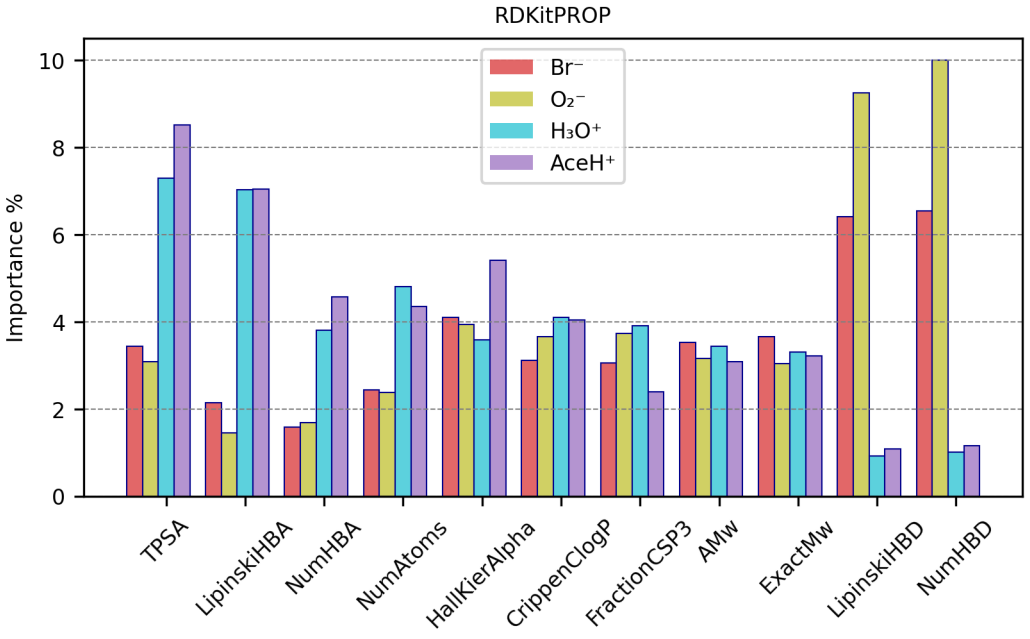

Figure 9. RDKitPROP RF best estimator features importance % of a subset of properties for each ionization method.

As mentioned in Sect. 3.1, some properties present repetitive information, which means that the overall importance relative to the number of HBD, as an example, is shared between the NumHBD property and the LipinskiHBD property. Either property probably would have reached a higher importance if only one of the two were considered. The other two properties that present repetitive information are the number of HBA (with importance shared between NumHBA and LipinskiHBA), and the molecular weight (with importance shared between AMw and ExactMw). Going into more detail, the number of HBD correlates strongly with negative ionization methods and the number of HBA with positive ones. This behaviour is expected, because HBD quantifies the number of hydrogen atoms attached to either oxygen or nitrogen atoms. Both of these groups can create a hydrogen bond and thus promote the interaction with negative reagent ions. Conversely, HBA encodes the number of oxygen or nitrogen atoms in the molecule, which can both create a hydrogen bond or accept a proton, promoting the interaction with positive reagent ions.

The high importance of TPSA highlights the significance of the molecular polar surface for the interaction with the reagent ions. As expected, if the polarity is right, the reagent ion can bind. The binding energy and thus the CIMS signal intensity

https://doi.org/10.5194/egusphere-2024-1846
Preprint. Discussion started: 18 July 2024

then increase with increasing polarity. Notably, our models assign a higher importance to the polarity for positive reagent ions, possibly due to the higher number of detected pesticides in the data. However, it is important to note that TPSA was originally calculated and implemented by not including halogen contributions in the equation (Ertl et al., 2000; Landrum, 2006). Therefore, the high presence of bromine, fluorine and iodine atoms in pesticides influences the polarity and might result in a different polar surface area.

Similar to TPSA, CrippenClogP adds the importance of hydrophilicity to the interaction list. The importance of the molecular weight and NumAtoms indicates that the molecular size correlates with detectability, possibly, because a larger molecule offers more van der Waals binding and potentially more binding sites for the reagent ion.

HallKierAlpha was also found useful in predicting molecular detection characteristics, which indicates that for each molecule the sum of the scaled measures of each atom's covalent radius (adjusted for its hybridization state relative to the covalent radius of a sp^3 hybridized carbon atom) relates to the reagent ion-target molecule interaction. For all ionization methods, both detected and undetected molecules have negative HallKierAlpha values (see Table S16 and Table S16), suggesting that the molecules in the dataset generally have smaller average atomic sizes relative to a sp^3 hybridized carbon atom. Detected molecules exhibit, on average, a smaller HallKierAlpha value than undetected ones. However, it is not clear, if this difference in HallKierAlpha values is statistically significant.

The presence of FractionCSP3 among the most important features indicates that the fraction of sp^3 hybridized carbons in the molecule contributes to the reagent ion-molecule interaction. With an in-depth analysis, the data suggests that molecules with a 'rigid' structure (fewer sp^3 carbons) slightly prefer interaction with negative reagent ions, while molecules with flexible structures (more sp^3 carbons) slightly prefer interaction with positive reagent ions.

Figure 10 reports the importance values in percentage of a representative subset of the 50 most important keys (e.g. reaching 1% importance for at least one ionization method) of the MACCS model for the four ionization methods (the remaining important keys can be found in Table S18 and Table S19 in the SI). We find no key with importance above 6%, suggesting that in complex systems such as pesticides, no single structural or chemical feature dominates the interaction with the reagent ions. Instead, multiple features of the molecule participate in the interaction, either by actively connecting to the reagent ion or passively through, e.g., inductive effects that increase the bond strength. It is also important to remember that our dataset is quite diverse. Thus, specific features or functional groups could have different importance for different types of molecules, decreasing the overall importance values. The groups with the highest importance are amines (NH, either primary or secondary) and hydroxyl (OH), for negative reagent ions, and nitrogen and nitrogen atoms with three single bonds (*NA(A)A*, where "A" stands for any element) for positive reagent ions. All other features do not surpass 2.5% of importance, on average.

https://doi.org/10.5194/egusphere-2024-1846
Preprint. Discussion started: 18 July 2024

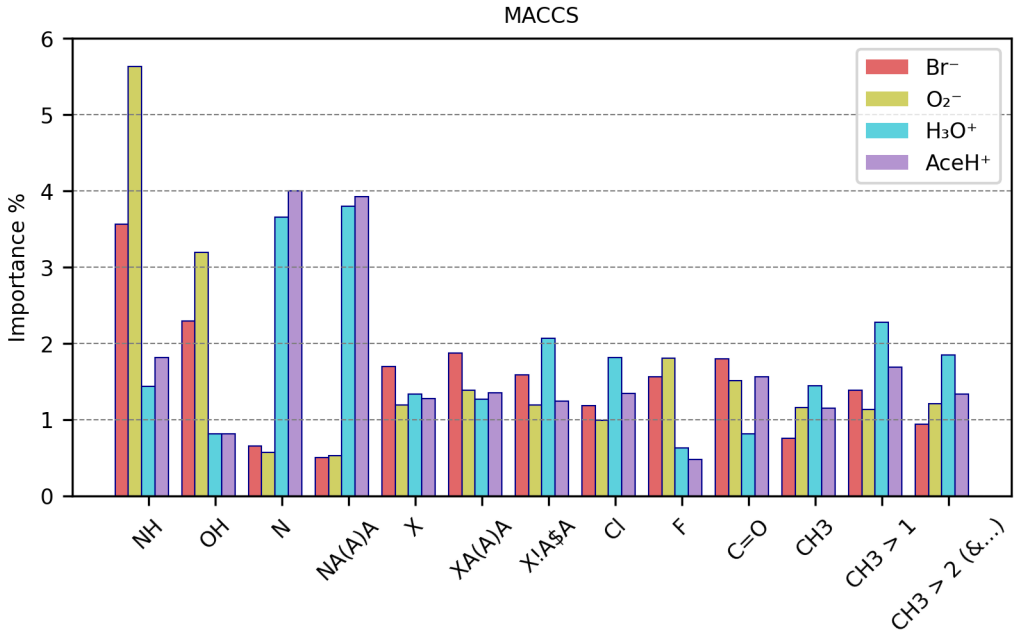

Figure 10. MACCS RF best estimator features importance % of a subset of MACCS keys for each ionization method.

Additionally, Table 4 reports a subset of the 50 most important MACCS features. The table reports individually for each reagent ion: the key (or group) structure, its importance value in (IMP %), the proportion of appearance in the dataset (PP %) and the average count of the appearing key per molecule (*Avg*) (calculated individually for detected (D) and undetected (ND) pesticides).

NH is most important for Br^- and $O_2{}^-$ (3.56% and 5.64% of importance respectively). It is nearly twice as important for detected than undetected pesticides (approx. 57% vs approx. 24%). With 2.29% and 3.19%, the importance of OH is slightly lower than for NH. Like NH, OH groups trigger predominately for detected pesticides (approx. 23% for detected vs 6% for undetected molecules). For both OH and NH groups, the undetected pesticides had a higher average frequency of appearance (*Avg*, how many times a group is present in a molecule, for the full dataset on average, by considering only the detected or undetected cases). However, we note that negative reagent ions suffer from a class imbalance, and the high amount of undetected cases could influence this statistic.

Both OH and NH are HBD groups. OH is known to be important for the interaction with negative reagent ions, while the importance of NH groups for this interaction has been observed by quantum chemical calculations in Partovi et al. (2023). With our ML models, we find these relations solely through patterns in the data.

For positive ionization schemes, OH groups do not reach 1% of importance and do not present any relevant variation between detected and undetected. Amine groups reach 1% of importance and correlate with detected pesticides (44% for detected vs 19% for undetected molecules). For $AceH^+$ ionization, NH is only the 4th most important feature. The most important

https://doi.org/10.5194/egusphere-2024-1846
Preprint. Discussion started: 18 July 2024

groups for positive ionization are instead those containing nitrogen. Being a HBA, nitrogen is an element that can facilitate the interaction between reagent ions and sample molecules.

The presence of nitrogen (N in the table) reaches 3.65% and 4.00% in importance for H_3O^+ and $AceH^+$. In both datasets, N appears approximately in 88% of the detected pesticides and in 52% of the undetected pesticides. Similarly, *NA(A)A* groups reach 3.80 % and 3.93 % of importance for H_3O^+ and $AceH^+$. This group is common in the studied dataset (for positive reagent ions: approximately 83% for detected, but only 42% for undetected pesticides).

Next, we will analyse other groups with importance for both positive and negative reagent ions. Five important features relate to the presence of halogens: the first three indicate if a halogen is present (*X*), if it has three single bonds (*XA(A)A*), and if it is bonded to a ring (*X!A$A*, where "!" stands for a chain or non-ring bond and "*$*" stands for a ring bond). The last two specify whether the halogen is a chlorine (Cl) or fluorine (F) atom. These halogen-related features range between 1% and 2% in importance across the four ionization schemes (F is the only one not reaching 1% of importance for positive reagent ions). For negative reagent ions, these groups are 10-20% more prevalent in detected than undetected pesticides. However, the average frequency of appearance per molecule between detected and undetected molecules does not present any clear difference. In contrast, molecules detected by positive reagent ions have 15-20% fewer halogen features than undetected molecules (specifically for the groups *X*, *XA(A)A*, *X!A$A*). The frequency of appearance per molecule is also higher for undetected pesticides, with an average of 3 to 6 groups per molecule (compared to 2-3 groups per molecule for detected instances). F shows the opposite trend for positive reagent ions. It has a slightly higher presence and a higher average group frequency for detected molecules. However, as previously stated, F does not reach 1% of importance for positive ionization schemes, so this result might not be as relevant as for the other features. In summary, the presence of halogens in a molecule enhances the detectability of negative ionization schemes and reduces it for positive ones.

The carbonyl group have a moderate importance (<2%) for all ionization schemes. For Br^- and O_2^-, the importance is 1.8% and 1.52% and for H_3O^+ and $AceH^+$ 0.82% and 1.57%, respectively. Focusing on negative reagent ions, C=O appears approximately in 70% of the detected pesticides and in 50% of the undetected ones, with a similar frequency per molecule (1.3 times). Carbonyl is an HBA group. Its importance for negative ionization schemes could therefore be due to either an inductive effect of oxygen or a possible redirection of the reagent ion to HBD groups. For positive reagent ions, C=O is present in approximately 64% detected and 40% undetected molecules, following its ability to accept hydrogens.

Among the important MACCS keys, we find three which enumerate whether there is one, more than one or more than two methyl groups (CH_3, CH_3>1 and CH_3>2). The positive ionization schemes show a greater prevalence of these features for detected pesticides than the negative schemes. For positive reagent ions, CH_3 is most important when it appears two times in a molecule.

https://doi.org/10.5194/egusphere-2024-1846
Preprint. Discussion started: 18 July 2024

Table 4. MACCS-based RF best estimator feature importances % of a subset of structural keys (groups). For each key, the structure, the importance value (IMP %) and the proportion of presence (PP%) with, in addition, the average group count per molecule (Avg) for detected (D) and undetected (ND) molecules are stated. In the name of the structures, the special characters stand for: "A": any element, "X": halogen, "!": chain or non-ring bond and "$": ring bond.

	Br^-					O_2^-				
		D		ND			D		ND	
Structure	IMP %	PP %	Avg	PP %	Avg	IMP %	PP %	Avg	PP %	Avg
NH	3.56	50.33	1.28	25.95	1.38	5.64	64.22	1.26	23.79	1.41
OH	2.29	21.00	1.02	6.11	1.25	3.19	24.77	1.02	6.95	1.18
N	0.66	83.67	2.39	71.50	2.05	0.57	87.16	2.41	72.00	2.10
NA(A)A	0.50	77.33	3.10	64.12	2.83	0.53	79.36	3.32	65.47	2.76
X	1.70	66.67	2.90	48.09	2.68	1.19	67.43	2.86	50.95	2.75
XA(A)A	1.87	64.33	3.43	43.00	3.60	1.38	64.68	3.33	46.53	3.63
X!A$A	1.59	54.00	4.13	36.39	4.94	1.19	53.67	3.79	39.58	4.95
Cl	1.18	53.33	1.94	40.20	2.37	0.99	50.46	1.72	43.79	2.38
F	1.56	25.67	3.34	10.43	2.56	1.81	28.90	3.48	11.58	2.60
C=O	1.80	68.33	1.34	50.38	1.32	1.52	72.48	1.31	51.58	1.34
CH_3	0.76	74.67	2.58	82.70	2.87	1.16	70.18	2.55	83.37	2.83
$CH_3 > 1$	1.39	56.00	3.10	71.50	3.16	1.14	53.21	3.04	70.11	3.17
$CH_3 > 2$ (&...)	0.94	35.00	3.76	43.77	3.90	1.21	29.82	3.86	44.63	3.84
	H_3O^+					$AceH^+$				
		D		ND			D		ND	
Structure	IMP %	PP %	Avg	PP %	Avg	IMP %	PP %	Avg	PP %	Avg
NH	1.44	44.68	1.29	19.28	1.49	1.82	44.94	1.28	18.26	1.58
OH	0.81	10.43	1.00	17.04	1.18	0.82	10.34	1.00	17.35	1.18
N	3.65	88.30	2.28	52.47	1.97	4.00	88.19	2.26	52.05	2.04
NA(A)A	3.80	82.98	2.87	42.15	3.31	3.93	82.91	2.88	41.55	3.29
X	1.33	49.15	2.41	70.85	3.36	1.27	50.42	2.44	68.49	3.36
XA(A)A	1.27	45.53	2.79	66.37	4.55	1.35	47.05	2.81	63.47	4.64
X!A$A	2.07	37.02	3.23	58.74	6.21	1.24	39.66	3.26	53.42	6.52
Cl	1.81	38.51	1.50	61.43	3.01	1.34	40.51	1.51	57.53	3.13
F	0.63	19.15	3.04	12.56	3.14	0.48	18.99	3.10	12.79	2.96
C=O	0.82	63.62	1.31	46.64	1.39	1.57	64.77	1.32	43.84	1.38
CH_3	1.44	85.96	2.90	65.02	2.34	1.15	84.81	2.86	67.12	2.44
$CH_3 > 1$	2.28	72.55	3.25	48.43	2.80	1.69	70.68	3.23	52.05	2.86
$CH_3 > 2$ (&...)	1.85	47.66	3.90	23.77	3.62	1.34	45.36	3.92	28.31	3.58

https://doi.org/10.5194/egusphere-2024-1846
Preprint. Discussion started: 18 July 2024

Overall, RDKitPROP and MACCS in combination with RF have given us insight into CIMS ion-molecule interactions, reaffirming general knowledge obtained by quantum chemical calculations or revealing uncharted features. Notably, our analysis extended to larger molecules than those examined by Partovi et al. (2023), demonstrating that the insights gained apply to a wider variety of molecules.

Given the simplicity of both molecular descriptors, minimal computational resources were needed to obtain the insight we discussed in this section. Compared to the computationally more demanding quantum chemical calculations, ML can more easily expose trends across different ionization schemes, distinguish between detected and undetected molecules and handle larger molecular sets and groups. However, for analyzing the interaction between specific reagent ions and molecules, quantum chemical computations still provide an advantage.

6 Conclusions

In summary, we developed a ML workflow for predicting the detection with CIMS (with a classification algorithm) and CIMS sensitivity to molecules (with a regression algorithm) to improve atmospheric compound identification. Two standard solutions containing 693 pesticides were analyzed with orbitrap TD-MION-MS. A RF classifier and a KRR model were trained on five different molecular structure representations. The best descriptor found is MACCS for both the classification and the regression. In the case of classification, MACCS reaches 0.85 $\pm$ 0.02 of accuracy and AUC of 0.91 $\pm$ 0.01; in the case of regression, MACCS can reach 0.44 $\pm$ 0.03 of MAE in logarithmic units of signal intensity. Models based on this descriptor have the lowest errors in both algorithms and are also easy to understand and implement, as they encode the presence of functional groups, or structural fragments starting from SMILES strings. Because of its white-box nature, the MACCS descriptor can provide chemical insight. Our feature importance analysis of the RF classifier provided insight into the reagent-ion interaction. RDKitPROP highlighted trends in the data that are generally known from basic chemical intuition. The feature analysis of the MACCS-based model highlighted the possible structural fragments that might impact the detection of the molecules. Models based on the two negative ionization methods, Br^- and $O_2{}^-$, presented similar results, such as the high importance of OH and NH groups, and carbonyls and halogens. Positive ionization methods, H_3O^+ and $AceH^+$, also presented similar results and highlighted the key role of nitrogen for detection and halogens for decreasing the chances of detection. These are the most relevant features found for the ML model, which generalizes features of experimental data. The results demonstrate that it is possible to extract sensible information even in small experimental datasets. However, more instances could help to generalize the structural features better and help prevent class imbalance problems.

The ML models developed in this work are a first step towards optimizing CIMS measurements for comprehensive reaction product detection with ML, aiming to enhance the general understanding of complex analyses such as that of atmospheric CIMS in the future. In future work, studying datasets with similar structures to atmospheric compounds (focusing on oxygenated compounds) could bring a greater understanding of the reagent ion and sample molecule interaction inside the instrumentation, thereby providing a greater understanding of the compounds detected in situ atmospheric measurement. An improvement in the ML performance could come from both experimental data and synthetic data. Furthermore, the development of standardized

https://doi.org/10.5194/egusphere-2024-1846
Preprint. Discussion started: 18 July 2024

experimental datasets is crucial, as these can significantly boost the possibility of using artificial intelligence algorithms and enhance the accuracy and reliability of future atmospheric analyses.

Code and data availability. The full dataset is freely available online at https://doi.org/10.5281/zenodo.11208543 (Partovi et al., 2024a). The ML methods implemented in this study are available on Gitlab.

Author contributions. FB prepared the manuscript, performed the analysis and validated the analysis. FB and HS curated the data, investigated the data and developed the model code. FB, HS, PR and MR contributed to the data visualization. HS and PR developed the methodology. HS, PR, and MR coordinated and supervised the project. MR acquired the funding for the project. FP and JM provided the experimental data. All authors reviewed and edited the manuscript.

Competing interests. Mario Simon, Siddharth Iyer and Matti Rissanen have several common papers through the cloud consortium. However, they have not worked closely for years anymore.

Acknowledgements. This project has received funding from the European Research Council under the European Union's Horizon 2020 research and innovation programme under Grant No. 101002728. The support from the Research Council of Finland (353836, 346373, 346377) and the European Cooperation in Science and Technology (CA22154) is greatly appreciated. We further acknowledge the CSC-IT Center for Science, Finland, and the Aalto Science-IT project. FB personally thanks Siddharth Iyer for the useful discussions on chemical ionization.

https://doi.org/10.5194/egusphere-2024-1846
Preprint. Discussion started: 18 July 2024

References

Besel, V., Todorović, M., Kurtén, T., Rinke, P., and Vehkamäki, H.: Atomic structures, conformers and thermodynamic properties of 32k atmospheric molecules, Scientific data, 10, 450, 2023.

Breiman, L.: Random Forests, Machine Learning, 45, 5–32, 2001.

Breitenlechner, M., Fischer, L., Hainer, M., Heinritzi, M., Curtius, J., and Hansel, A.: PTR3: An Instrument for Studying the Lifecycle of Reactive Organic Carbon in the Atmosphere, Analytical Chemistry, 89, 5824–5831, https://doi.org/10.1021/acs.analchem.6b05110, 2017.

Brouard, C., Shen, H., Dührkop, K., D'Alché-Buc, F., Böcker, S., and Rousu, J.: Fast metabolite identification with Input Output Kernel Regression, Bioinformatics, 32, i28–i36, https://doi.org/10.1093/BIOINFORMATICS/BTW246, 2016.

Brüggemann, M., Mayer, S., Brown, D., Terry, A., Rüdiger, J., and Hoffmann, T.: Measuring pesticides in the atmosphere: current status, emerging trends, and future perspectives, Environmental Sciences Europe, 36, https://doi.org/10.1186/s12302-024-00870-4, 2024.

de Gouw, J. and Warneke, C.: Measurements of volatile organic compounds in the earth's atmosphere using proton-transfer-reaction mass spectrometry, Mass Spectrometry Reviews, 26, 223–257, https://doi.org/10.1002/mas.20119, 2007.

Durant, J. L., Leland, B. A., Henry, D. R., and Nourse, J. G.: Reoptimization of MDL Keys for Use in Drug Discovery, Journal of Chemical Information and Computer Sciences, 42, 1273–1280, 2002.

Dührkop, K., Shen, H., Meusel, M., Rousu, J., and Böcker, S.: Searching molecular structure databases with tandem mass spectra using CSI:FingerID, Proceedings of the National Academy of Sciences of the United States of America, 112, 12 580–12 585, https://doi.org/10.1073/PNAS.1509788112/SUPPL_FILE/PNAS.201509788SI.PDF, 2015.

Eisele, F. L. and Tanner, D. J.: Measurement of the gas phase concentration of H2SO4 and estimates of H2SO4 production and loss in the atmosphere, Journal of Geophysical Research: Atmospheres, 98, 9001–9010, https://doi.org/10.1029/93JD00031, 1993.

Erban, A., Fehrle, I., Martinez-Seidel, F., Brigante, F., Más, A. L., Baroni, V., Wunderlin, D., and Kopka, J.: Discovery of food identity markers by metabolomics and machine learning technology, Scientific Reports, 9, https://doi.org/10.1038/s41598-019-46113-y, 2019.

Ertl, P., Rohde, B., and Selzer, P.: Fast Calculation of Molecular Polar Surface Area as a Sum of Fragment-Based Contributions and Its Application to the Prediction of Drug Transport Properties, Journal of Medicinal Chemistry, 43, 3714–3717, https://doi.org/10.1021/jm000942e, 2000.

GALAB: Galab Laboratories, Hamburg, Germany, https://www.galab.com/, accessed: 2024-06-04.

Géron, A.: Hands-On Machine Learning with Scikit-Learn, Keras, and TensorFlow: Concepts, Tools, and Techniques to Build Intelligent Systems, 1 edn., 2022.

Gitlab: PesticidesMS, https://gitlab.com/cest-group/pesticidesms, 2024.

Griffiths, J. R. and de Hoffmann, E.: Mass Spectrometry: Principles and Applications, John Wiley & Sons, 3rd edn., ISBN 9780470033104, 2007.

Hall, L. H. and Kier, L. B.: The Molecular Connectivity Chi Indexes and Kappa Shape Indexes in Structure-Property Modeling, chap. 9, pp. 367–422, Wiley-VCH, Inc., New York, 1991.

Heinonen, M., Shen, H., Zamboni, N., and Rousu, J.: Metabolite identification and molecular fingerprint prediction through machine learning, Bioinformatics, 28, 2333–2341, https://doi.org/10.1093/BIOINFORMATICS/BTS437, 2012.

Himanen, L., Jäger, M. O., Morooka, E. V., Canova, F. F., Ranawat, Y. S., Gao, D. Z., Rinke, P., and Foster, A. S.: DScribe: Library of descriptors for machine learning in materials science, Computer Physics Communications, 247, 106 949, https://doi.org/10.1016/j.cpc.2019.106949, 2020.

https://doi.org/10.5194/egusphere-2024-1846
Preprint. Discussion started: 18 July 2024

Hoerl, A. E. and Kennard, R. W.: Ridge Regression: Biased Estimation for Nonorthogonal Problems, Technometrics, 12, 55–67, https://doi.org/10.1080/00401706.1970.10488634, 1970.

Houde, M., Wang, X., Colson, T.-L. L., Gagnon, P., Ferguson, S. H., Ikonomou, M. G., Dubetz, C., Addison, R. F., and Muir, D. C. G.: Trends of persistent organic pollutants in ringed seals (Phoca hispida) from the Canadian Arctic, Science of The Total Environment, 665, 1135–1146, https://doi.org/10.1016/j.scitotenv.2019.02.138, 2019.

Huey, L. G.: Measurement of trace atmospheric species by chemical ionization mass spectrometry: Speciation of reactive nitrogen and future directions, Mass Spectrometry Reviews, 26, 166–184, https://doi.org/10.1002/mas.20118, 2007.

Huo, H. and Rupp, M.: Unified representation of molecules and crystals for machine learning, Machine Learning: Science and Technology, 3, https://doi.org/10.1088/2632-2153/aca005, 2022.

Hyttinen, N., Otkjær, R. V., Iyer, S., Kjaergaard, H. G., Rissanen, M. P., Wennberg, P. O., and Kurtén, T.: Computational Comparison of Different Reagent Ions in the Chemical Ionization of Oxidized Multifunctional Compounds, Journal of Physical Chemistry A, 122, 269–279, https://doi.org/10.1021/acs.jpca.7b10015, 2018.

Iyer, S., Lopez-Hilfiker, F., Lee, B. H., Thornton, J. A., and Kurtén, T.: Modeling the Detection of Organic and Inorganic Compounds Using Iodide-Based Chemical Ionization, Journal of Physical Chemistry A, 120, https://doi.org/10.1021/acs.jpca.5b09837, 2016.

James, C., Weininger, D., and Delany, J.: Daylight Theory Manual. Daylight Chemical Information Systems, 1995.

Karsa: Karsa Oy, https://karsa.fi/, accessed: 2024-06-04.

Krishnamurthy, R., Newsom, R. K., Berg, L. K., Xiao, H., Ma, P.-L., and Turner, D. D.: On the estimation of boundary layer heights: a machine learning approach, Atmospheric Measurement Techniques, 14, 4403–4424, https://doi.org/10.5194/amt-14-4403-2021, 2021.

Laakso, J., Himanen, L., Homm, H., Morooka, E. V., Jäger, M. O., Todorović, M., and Rinke, P.: Updates to the DScribe library: New descriptors and derivatives, The Journal of Chemical Physics, 158, 2023.

Landrum, G.: RDKit: Open-Source Cheminformatics Software, http://www.rdkit.org, accessed: 2024-06-04, 2006.

Langer, M. F., Goeßmann, A., and Rupp, M.: Representations of molecules and materials for interpolation of quantum-mechanical simulations via machine learning, npj Comput Mater, 8, https://doi.org/10.1038/s41524-022-00721-x, 2022.

Laskin, J., Laskin, A., and Nizkorodov, S. A.: Mass Spectrometry Analysis in Atmospheric Chemistry, Analytical Chemistry, 90, 166–189, https://doi.org/10.1021/acs.analchem.7b04249, 2018.

Lumiaro, E., Todorović, M., Kurten, T., Vehkamäki, H., and Rinke, P.: Predicting gas–particle partitioning coefficients of atmospheric molecules with machine learning, Atmos. Chem. Phys., 21, https://doi.org/10.5194/acp-21-13227-2021, 2021.

Munson, B.: Chemical Ionization Mass Spectrometry, Analytical Chemistry, 43, 28–37, https://doi.org/DOI not provided in the document, 1971.

Munson, B.: Chemical Ionization Mass Spectrometry: Theory and Applications, in: Encyclopedia of Analytical Chemistry, pp. 1–18, John Wiley & Sons, Ltd, https://doi.org/10.1002/9780470027318.a6004, 2006.

Munson, M. S. B. and Field, F. H.: Chemical Ionization Mass Spectrometry: I. General Introduction, Journal of the American Chemical Society, 88, 2621–2630, https://doi.org/10.1021/ja00960a001, 1966.

Nguyen, D. H., Nguyen, C. H., and Mamitsuka, H.: SIMPLE: Sparse Interaction Model over Peaks of moLEcules for fast, interpretable metabolite identification from tandem mass spectra, Bioinformatics, 34, i323–i332, https://doi.org/10.1093/BIOINFORMATICS/BTY252, 2018.

https://doi.org/10.5194/egusphere-2024-1846
Preprint. Discussion started: 18 July 2024

Nguyen, D. H., Nguyen, C. H., and Mamitsuka, H.: Recent advances and prospects of computational methods for metabolite identification: a review with emphasis on machine learning approaches, Briefings in Bioinformatics, 20, 2028–2043, https://doi.org/10.1093/BIB/BBY066, 2019.

Partovi, F., Mikkilä, J., Iyer, S., Mikkilä, J., Kontro, J., Ojanperä, S., Juuti, P., Kangasluoma, J., Shcherbinin, A., and Rissanen, M.: Pesticide Residue Fast Screening Using Thermal Desorption Multi-Scheme Chemical Ionization Mass Spectrometry (TD-MION MS) with Selective Chemical Ionization, ACS Omega, 8, 25 749–25 757, 2023.

Partovi, F., Bortolussi, F., Mikkilä, J., and Rissanen, M.: Organic pesticide database with 716 molecules analyzed with chemical ionization mass spectrometry. Reagent ions: bromide, protonated acetone, hydronium ion, dioxide., https://doi.org/10.5281/zenodo.11208543, 2024a.

Partovi, F., Mikkilä, J., Iyer, S., Mikkilä, J., Kontro, J., Ojanperä, S., Shcherbinin, A., and Rissanen, M.: Multi-Scheme Chemical Ionization for Pesticide Detection: A MION-Orbitrap Mass Spectrometry Study, Manuscript in preparation, 2024b.

Pedregosa, F., Varoquaux, G., Gramfort, A., Michel, V., Thirion, B., Grisel, O., Blondel, M., Prettenhofer, P., Weiss, R., Dubourg, V., Vanderplas, J., Passos, A., Cournapeau, D., Brucher, M., Perrot, M., and Duchesnay, E.: Scikit-learn: Machine Learning in Python, Journal of Machine Learning Research, 12, 2825–2830, 2011.

Rissanen, M. P., Mikkilä, J., Iyer, S., and Hakala, J.: Multi-scheme chemical ionization inlet (MION) for fast switching of reagent ion chemistry in atmospheric pressure chemical ionization mass spectrometry (CIMS) applications, Atmospheric Measurement Techniques, 12, 6635–6646, 2019.

Riva, M., Rantala, P., Krechmer, J. E., Peräkylä, O., Zhang, Y., Heikkinen, L., Garmash, O., Yan, C., Kulmala, M., Worsnop, D., and Ehn, M.: Evaluating the performance of five different chemical ionization techniques for detecting gaseous oxygenated organic species, Atmospheric Measurement Techniques, 12, 2403–2421, https://doi.org/10.5194/amt-12-2403-2019, 2019.

Rupp, M.: Machine Learning for Quantum Mechanics in a Nutshell, International Journal of Quantum Chemistry, 115, 1058–1073, https://doi.org/10.1002/qua.24954, 2015.

Rupp, M., Tkatchenko, A., Müller, K.-R., and von Lilienfeld, O. A.: Fast and Accurate Modeling of Molecular Atomization Energies with Machine Learning, Physical Review Letters, 108, 1–5, 2012.

Sandström, H., Rissanen, M., Rousu, J., and Rinke, P.: Data-Driven Compound Identification in Atmospheric Mass Spectrometry, Advanced Science, 11, 2023.

Siomos, N., Fountoulakis, I., Natsis, A., Drosoglou, T., and Bais, A.: Automated Aerosol Classification from Spectral UV Measurements Using Machine Learning Clustering, Remote Sensing, 12, 965, https://doi.org/10.3390/rs12060965, 2020.

Sipilä, M., Sarnela, N., Jokinen, T., Henschel, H., Junninen, H., Kontkanen, J., Richters, S., Kangasluoma, J., Franchin, A., Peräkylä, O., Rissanen, M. P., Ehn, M., Vehkamäki, H., Kurten, T., Berndt, T., Petäjä, T., Worsnop, D., Ceburnis, D., Kerminen, V.-M., Kulmala, M., and O'Dowd, C.: Molecular-scale evidence of aerosol particle formation via sequential addition of HIO3, Nature, 537, 532–534, https://doi.org/10.1038/nature19314, 2016.

Stuke, A., Todorović, M., Rupp, M., Kunkel, C., Ghosh, K., Himanen, L., and Rinke, P.: Chemical diversity in molecular orbital energy predictions with kernel ridge regression, The Journal of Chemical Physics, 150, 204 121, https://doi.org/10.1063/1.5086105, 2019.

Stuke, A., Rinke, P., and Todorović, M.: Efficient hyperparameter tuning for kernel ridge regression with Bayesian optimization, Machine Learning: Science and Technology, 2, 035 022, https://doi.org/10.1088/2632-2153/abee59, 2021.

Su, P., Joutsensaari, J., Dada, L., Zaidan, M. A., Nieminen, T., Li, X., Wu, Y., Decesari, S., Tarkoma, S., Petäjä, T., Kulmala, M., and Pellikka, P.: New particle formation event detection with Mask R-CNN, Atmospheric Chemistry and Physics, 22, 1293–1309, https://doi.org/10.5194/acp-22-1293-2022, 2022.

https://doi.org/10.5194/egusphere-2024-1846
Preprint. Discussion started: 18 July 2024

Thoma, M., Bachmeier, F., Gottwald, F. L., Simon, M., and Vogel, A. L.: Mass spectrometry-based *Aerosolomics*: a new approach to resolve sources, composition, and partitioning of secondary organic aerosol, Atmospheric Measurement Techniques, 15, 7137–7154, https://doi.org/10.5194/amt-15-7137-2022, 2022.

van der Maaten, L. and Hinton, G.: Visualizing Data using t-SNE, Journal of Machine Learning Research, 9, 2579–2605, http://jmlr.org/papers/v9/vandermaaten08a.html, 2008.

Wildman, S. A. and Crippen, G. M.: Prediction of Physicochemical Parameters by Atomic Contributions, Journal of Chemical Information and Computer Sciences, 39, 868–873, https://doi.org/10.1021/ci990307l, 1999.

Xue, L. and J, J. B.: Molecular descriptors in chemoinformatics, computational combinatorial chemistry, and virtual screening, Comb Chem High Throughput Screen, 8, https://doi.org/10.2174/1386207003331454, 2020.